

PAPER

Electric field control of spin-orbit torque in annealed Ta/CoFeB/HfO_x heterostructures via interfacial oxidation modulation

To cite this article: Shuo Wu *et al* 2024 *Nanotechnology* **35** 365205

View the [article online](#) for updates and enhancements.

You may also like

- [Thermal Robustness of VFB and EOT in HfO_x\(N\) p-MOS Devices with Partially Silicided Pt Gate Electrodes](#)
Masaru Kadoshima, Toshihide Nabatame, Masashi Takahashi *et al.*
- [Synaptic transistor with a reversible and analog conductance modulation using a Pt/HfO_x/n-IGZO memcapacitor](#)
Paul Yang, Hyung Jun Kim, Hong Zheng *et al.*
- [Modulation of the Electrical Characteristics of HfO_x/TiN RRAM Devices Through the Top Electrode Metal](#)
Kow-Ming Chang, Wen-Hsien Tzeng, Kou-Chen Liu *et al.*



The Electrochemical Society

Advancing solid state & electrochemical science & technology

DISCOVER
how sustainability
intersects with
electrochemistry & solid
state science research



Electric field control of spin-orbit torque in annealed Ta/CoFeB/HfO_x heterostructures via interfacial oxidation modulation

Shuo Wu¹, Tianli Jin, Calvin Ching Ian Ang, Gerard Joseph Lim¹, Bryan Wei Hao Cheng, Ze Chen and Wen Siang Lew*¹

School of Physical and Mathematical Sciences, Nanyang Technological University, 21 Nanyang Link, Singapore 637371, Singapore

E-mail: wensiang@ntu.edu.sg

Received 20 January 2024, revised 29 May 2024

Accepted for publication 11 June 2024

Published 21 June 2024



Abstract

Electric field control of spin-orbit torque (SOT) exhibits promising potential in advanced spintronic devices through interfacial modulation. In this work, we investigate the influence of electric field and interfacial oxidation on SOT efficiency in annealed Ta/CoFeB/HfO_x heterostructures. By varying annealing temperatures, the damping-like SOT efficiency reaches its peak at the annealing temperature of 320 °C, with an 80% field-free magnetization switching ratio induced by SOT having been demonstrated. This enhancement is ascribed to the annealing-induced modulation of oxygen ion migration at the CoFeB/HfO_x interface. By applying voltages across the Ta/CoFeB/HfO_x heterostructures, which drives the O²⁻ migration across the interface, a reversible, bipolar, and non-volatile modulation of SOT efficiency was observed. The collective influence of annealing temperature and electric field effects on SOT carried out in this work provides an effective approach into facilitating the optimization and control of SOT in spintronic devices.

Supplementary material for this article is available [online](#)

Keywords: spintronics, voltage-controlled spin-orbit torque, interfacial oxidation

1. Introduction

Spin-orbit torque (SOT) has emerged as a highly promising and efficient method for magnetization switching in spintronic devices, offering potential advantages in low-power logic and memory applications [1, 2]. To improve SOT efficiency, various approaches have been proposed, such as using different heavy metals and metallic alloys [3–5], optimizing insertion layers with varying thicknesses [6–8], and modulating the heavy metal (HM)/ferromagnet (FM) interface

[9–11]. Additionally, interfacing with an oxide layer has been found to play a crucial role in modifying the magnetic anisotropy of ferromagnetic layers. The degree of interfacial oxidation significantly influences the electronic structure and the strength of spin-orbit coupling [12, 13]. Moreover, electric field has been identified as an effective approach to modify magnetic properties, including magnetic anisotropy, coercivity, Curie temperature, magnetoresistance, and spin-orbit fields [14–19]. By applying gate voltages, it becomes possible to control the degree of oxidation in the magnetic material, leading to distinct magneto-ionic regimes [12]. This gate-voltage-induced oxidation process offers a promising way to manipulate interfacial properties and, consequently,

* Author to whom any correspondence should be addressed.

modulate SOT efficiency in a controllable and reversible manner. Notably, voltage control of SOT has been demonstrated in various systems, such as the Pt/Co system [20, 21], a Cr-doped topological insulator [22], and using ionic liquid [12, 23]. Previous works [24–26] primarily utilized electric fields to influence interfacial oxidation in voltage-controlled magnetism within ferromagnetic/oxide systems, thereby facilitating magnetization switching through changes in magnetic properties. However, other factors such as annealing temperature, can also affect interfacial oxygen migration and should be jointly investigated with electric fields to observe potential enhancements or modulations in SOT. A comprehensive understanding of oxidation's role and behavior at the interface through various potential influencing factors is crucial for unraveling the underlying mechanisms of voltage-controlled SOT [27].

In this work, we investigated the influence of electric field and interfacial oxidation on SOT in Ta/CoFeB/HfO_x heterostructures. Through annealing the thin film stack at different temperatures, we observed variations in coercivity, saturation magnetization, and the damping-like and field-like effective field efficiency. SOT efficiency improved with increasing annealing temperatures, with an 80% field-free magnetization switching ratio demonstrated. This enhancement can be attributed to an increased oxidation state of Co and Fe, as well as an increased spin-orbit coupling strength [28]. Additionally, by applying voltages across the Ta/CoFeB/HfO_x heterostructures which allows for interfacial oxygen ion modulation, we investigated the reversible modulation of SOT efficiency through the control of oxidation levels at the CoFeB/HfO_x interface. We observed diminished effects on voltage-controlled SOT for samples annealed at higher temperature, which we attribute to their different post-annealing oxidation levels. Our findings contribute to the understanding of interfacial oxidation and the electric field control of SOT, offering potential implications in the development of energy-efficient spintronic devices.

2. Experimental methods

A structure comprising Ta (5 nm)/CoFeB (1.2 nm)/HfO_x (2 nm) was prepared on a thermally oxidized Si substrate. All the layers were deposited by using magnetron sputtering at room temperature with a base pressure of 5×10^{-8} Torr. Thermal annealing was carried out in ultra-high vacuum for 60 mins. The magnetic hysteresis of the films was measured by using vibrating sample magnetometer (VSM). Hall cross devices of $10 \mu\text{m} \times 100 \mu\text{m}$ were fabricated using electron-beam lithography and argon ion milling techniques. Contact pads comprising of Ti (10 nm)/Cu (50 nm)/Ti (10 nm) were fabricated using a lift-off process. The magnetic properties of the devices were determined through electrical characterization via anomalous Hall effect measurements. The SOT efficiency was determined by measuring the harmonic Hall voltages using a Keithley 6221 AC current source and a 7265 Dual-Phase DSP Lock-In Amplifier [29].

3. Results and discussion

Figure 1(a) shows the magnetic hysteresis ($M-H_z$) loops of the post-annealed thin films by sweeping the magnetic field (H_z) along the out-of-plane direction. The hysteresis loops indicate the presence of perpendicular magnetic anisotropy (PMA) after thermal annealing with temperatures (T_a) from 200 °C to 360 °C. The hysteresis loops of the annealed samples display a step-like drop in coercivity (H_c) as the annealing temperature increases from 280 °C to 320 °C, as shown in figure 1(b). The saturation magnetization (M_s) gradually decays and approaches the value of 480 emu cm^{-3} when $T_a = 360$ °C. The observed decrease in M_s in the annealed samples can be attributed primarily to the oxidation of the CoFeB layer that forms the oxidized CoFe compounds [8], reducing the total magnetic moment of the CoFeB layer. Furthermore, after higher temperature annealing, more oxygen from the HfO_x layer migrates into the CoFeB layer due to the high oxygen ionic mobility [30].

Subsequently, the annealed Ta/CoFeB/HfO_x films were fabricated into $10 \mu\text{m} \times 100 \mu\text{m}$ Hall cross device structures. Note that the film annealed at 200 °C was unable to maintain the desired PMA after device fabrication (the discussion is included in supplementary material S1), and was omitted from the subsequent investigation. Figure 2(a) shows the Hall voltage measurement schematic with the applied in-plane magnetic fields along H_x and H_y . Figure 2(b) shows the anomalous Hall resistance $R_{\text{AHE}}-H_z$ loops of the measured Hall cross devices with different annealing temperatures. Aligned with the hysteresis loops behavior of their thin films, the devices with higher T_a have a reduced coercivity compared to the devices with lower T_a . The differences in H_c between Hall and VSM measurements can be linked to the energy needed for domain wall nucleation and motion during magnetization reversal. In thin films, random defects allow small fields to initiate domain wall motion. When these films are patterned into micro-sized devices, some defects are removed, creating more ordered magnetic domains. As a result, device-level samples need more energy to effectively nucleate and move domain walls, increasing H_c in Hall measurements compared to VSM measurements. To evaluate the damping-like and field-like field efficiency as a function of T_a , the first harmonic Hall voltage ($V_{1\omega}$) and second harmonic Hall voltage ($V_{2\omega}$) measurements were carried out by sweeping an external in-plane magnetic field in two directions: along the current direction (x -direction) and transverse to the current direction (y -direction). Based on the measured Hall voltage results, the damping-like field and field-like field are obtained from equation (1) [29]:

$$H_{\text{DL(F)}} = -2 \frac{H_{L(T)} \pm 2\xi H_{T(L)}}{1 - 4\xi^2}, \quad (1)$$

where H_L and H_T are defined as $H_{L,\pm} = (dV_{2\omega,x\pm}/dH_x)/(d^2V_{1\omega,x\pm}/dH_x^2)$ and $H_{T,\pm} = (dV_{2\omega,y\pm}/dH_y)/(d^2V_{1\omega,y\pm}/dH_y^2)$, respectively. ξ is the ratio of planar Hall resistance and

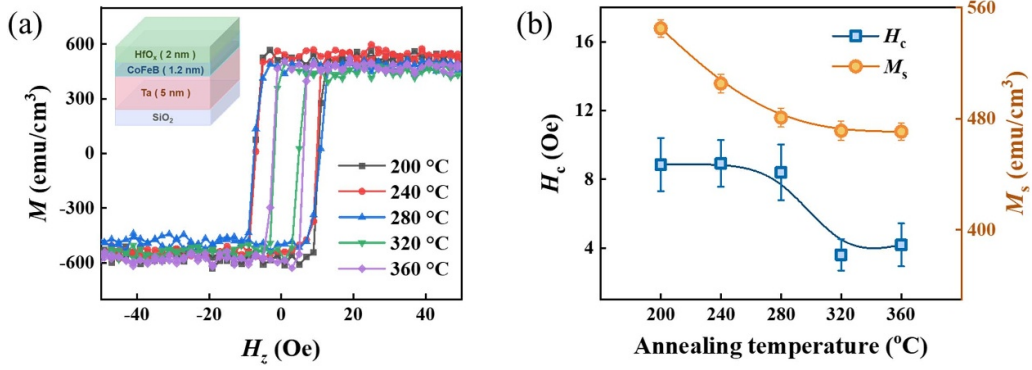


Figure 1. (a) Out-of-plane hysteresis loops and schematic illustration of Ta/CoFeB/HfO_x film. (b) The coercivity H_c and the saturation magnetization M_s under different annealing temperatures in Ta/CoFeB/HfO_x heterostructures.

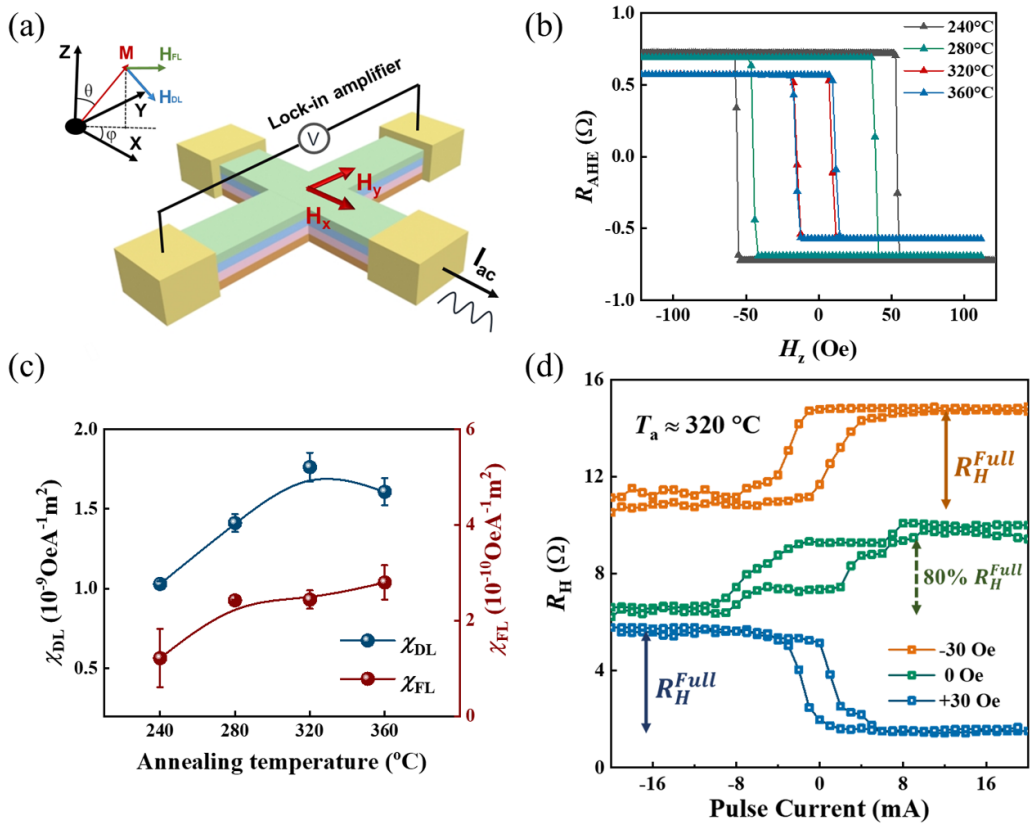


Figure 2. (a) Schematic of the Hall voltage measurement setup by sweeping in-plane field in longitudinal direction H_x and transverse direction H_y . (b) Anomalous Hall resistance loops measured on the annealed Ta/CoFeB/HfO_x devices under an out-of-plane field. (c) The damping-like field SOT efficiency χ_{DL} and the field-like field SOT efficiency χ_{FL} dependence on the annealing temperature for the Ta/CoFeB/HfO_x devices. (d) Current-induced magnetization switching of the 320 °C annealed sample under the external in-plane magnetic field of ± 30 Oe and 0 Oe.

anomalous Hall resistance (R_{PHE}/R_{AHE}). By fitting the experimental Hall voltage results under different current densities J_{ac} between 5×10^{10} and 9×10^{10} A m⁻², the corresponding damping-like field (H_{DL}) and field-like field (H_{FL}) were obtained (the details are shown in supplementary material S2). By fixing the intercept at zero and linearly fitting H_{DL} vs. J_{ac} , the damping-like effective field efficiency and the field-like effective field efficiency were derived as $\chi_{DL/FL} = H_{DL/FL}/J_{ac}$. Figure 2(c) shows the dependence of the χ_{DL} and χ_{FL} on

the annealing temperature. The χ_{DL} shows an increase with increasing T_a , peaking at around $(1.7 \pm 0.3) \times 10^{-9}$ Oe (A m⁻²)⁻¹ ($T_a = 320$ °C), which is 70% higher than the 240 °C annealed sample of $(1.0 \pm 0.1) \times 10^{-9}$ Oe (A m⁻²)⁻¹. The χ_{FL} exhibits an increase as T_a increases, reaching a maximum value of $(2.8 \pm 0.4) \times 10^{-10}$ Oe (A m⁻²)⁻¹. A higher annealing temperature can increase the damping-like and field-like effective field efficiency in the Ta/CoFeB/HfO_x stack due to the enhanced oxidation level. The annealing process

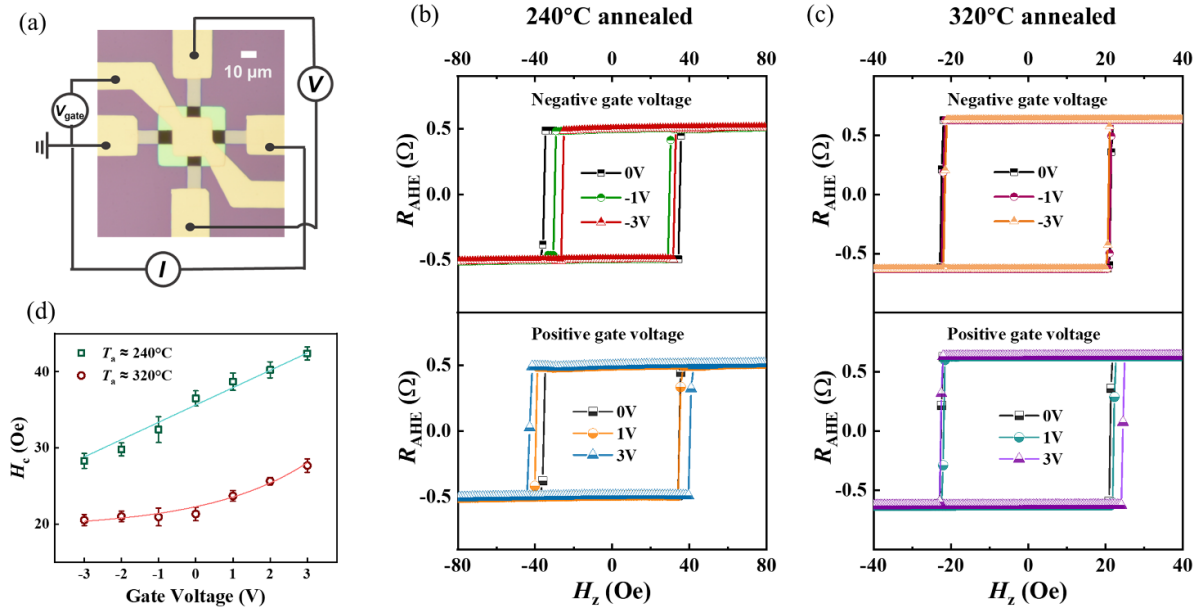


Figure 3. (a) Optical micrograph of the gated Hall bar device. I is the applied current into the Hall cross. V is the measured Hall voltage in the crossbar. V_{gate} is the applied gate voltage. (b) Anomalous Hall resistance measured under different negative and positive gate voltages with an out-of-plane magnetic field for devices annealed at (b) 240 °C and (c) 320 °C. (d) Coercivity H_c dependence on the gate voltage V_{gate} for the devices.

promotes the interdiffusion and interfacial mixing between the layers. At higher T_a , the formation of crystalline structures with reduced defects and interfacial roughness facilitates an efficient transmission of spin current across the interfaces [31–34]. Moreover, after annealing under a higher temperature, the migration of oxygen atoms from HfO_x into the CoFeB layers occurs. This migration leads to the formation of an enhanced oxidation state of Co and Fe, which enhances the spin current transmission and the interfacial Rashba effect at the CoFeB/ HfO_x interface [35–38]. Subsequent to the SOT measurement, the current-induced magnetization switching (CIMS) of the 320 °C annealed sample was carried out. The CIMS loops, which were measured using a series of DC current pulses under an external in-plane magnetic fields of ± 30 Oe and 0 Oe, are shown in figure 2(d). The pulse current was applied along the x -direction with a maximum magnitude of 18 mA and a duration of 5 ms. The CIMS loops exhibit full switching under a ± 30 Oe field, and an 80% field-free magnetization switching ratio is achieved. This is based on comparing the change in resistance due to magnetization switching without an external magnetic field ($\Delta R_{\text{field-free}}$) to the change in resistance when the magnetization is fully switched with the help of an external field (ΔR_{full}). The switching ratio, which is determined by $(\Delta R_{\text{field-free}}/\Delta R_{\text{full}}) \times 100\%$, reached 80%. This indicates that our device achieves substantial magnetization switching solely through SOT, without external magnetic assistance. This efficiency is crucial for developing energy-efficient spintronic devices that operate without the need for additional magnetic field components.

To further investigate how interfacial oxidation at the CoFeB/ HfO_x interface affects SOT efficiency, devices were fabricated for the voltage-gated measurement. This involved

the fabrication process of depositing an additional HfO_x with a thickness of 50 nm on top of the Hall cross structure to serve as the dielectric layer, followed by Ti (10 nm)/Cu (50 nm)/Ti (10 nm) deposited as a gate electrode. The configuration and electrical measurement setup of the voltage-gated device is illustrated in figure 3(a). It shows an optical micrograph of the gated Hall cross device. Note that the utilization of negative gate voltages results in the formation of an electric field that facilitates the downward migration of O^{2-} ions from the HfO_x layer into the CoFeB layer, vice versa [39]. To exemplify the electric field effect, the samples annealed at 240 °C and 320 °C with the largest difference in SOT efficiency were selected for gating measurements. The R_{AHE} was measured under various gate voltages, i.e. from $0 \rightarrow -3 \rightarrow 0 \rightarrow 3$ V. For the sample anneal at 240 °C as shown in figure 3(b), the R_{AHE} loops illustrate a reduction in H_c from 36 to 28 Oe under negative gate voltages. Under increasing the V_{gate} from 0 to 3 V, H_c gradually increases. For the sample annealed at 320 °C, as shown in figure 3(c), the R_{AHE} loop remains nearly unchanged under negative gate voltages. However, when positive gate voltages are applied, it exhibits a similar trend to that of the 240 °C annealed sample, with an increase in H_c . The gate voltage dependence of H_c for the samples annealed at 240 °C and 320 °C is shown in figure 3(d). The more pronounced electric field effects under gate voltages between the 240 °C and 320 °C annealed samples is attributed to the different post-annealing oxidation levels of Co and Fe [40, 41]. The 320 °C annealed sample has a saturated initial oxidation level, rendering it largely unaffected by negative gate voltages. Moreover, to evaluate the nonvolatility of the gate effect, a -3 V gate voltage was applied for 10 min and subsequently switched off. There was no discernible alterations observed in

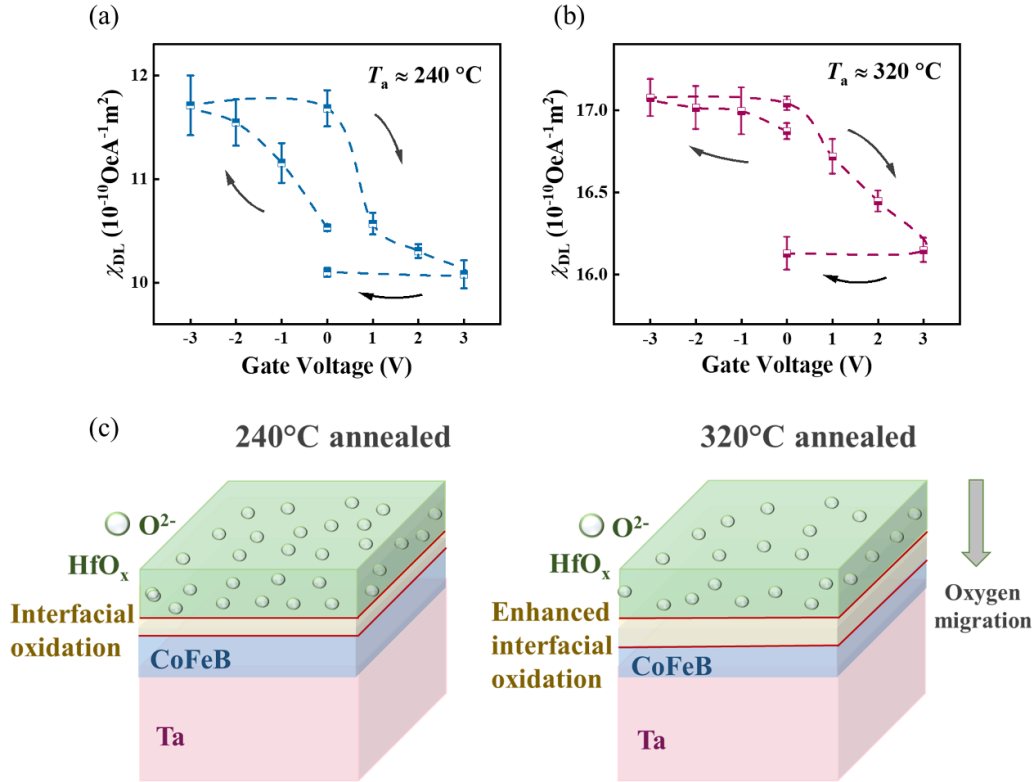


Figure 4. The damping-like field SOT efficiency χ_{DL} at different gate voltages V_{gate} for the devices annealed at (a) 240 °C and (b) 320 °C. (c) Schematic illustration of interfacial oxidation states at the CoFeB/HfO_x interface under different annealing temperatures.

the R_{AHE} vs. H_z curves between $V_{gate} = -3$ V and $V_{gate} = 0$ V (-3 V \rightarrow 0 V).

Subsequently, the dependence of the damping-like field SOT efficiency (χ_{DL}) on the applied gate voltages was measured, as shown in figures 4(a) and (b). The black arrows indicate the sequence of applied gate voltages. Dashed lines are a guide to the eye. The measurements under $V_{gate} = 0$ V demonstrates the nonvolatility of the electric field effect. For the samples annealed at 240 °C, χ_{DL} decreased under positive V_{gate} and increased under negative V_{gate} , with a variation of 16%. Aligned with the trend in H_c of the samples annealed at 320 °C, χ_{DL} also shows a minimal change under negative V_{gate} . Under a positive V_{gate} , χ_{DL} still decreases with increasing gate voltage, but with a smaller variation of 6%. The enhancement and diminishment of χ_{DL} under different gate voltage polarity observed here aligns closely with the voltage-driven control of the CoFeB layer's oxidation across the CoFeB/HfO_x interface. The formation of Co and Fe oxides, which modulates the hybridization of Co and Fe 3d orbitals and enhance the SOT efficiency [42, 43]. For the field-like SOT efficiency (χ_{FL}), we observed that the influence of voltage control was minimal for devices annealed at both 240 °C and 320 °C (the details are shown in supplementary material S4).

We attribute the distinct responses of gate voltage control of SOT efficiency to the oxidation level in the post-annealed samples. The migration of O²⁻ to the CoFeB layer is gradually enhanced with increasing annealing temperature, as illustrated

in figure 4(c). This figure demonstrates the oxidation level for the post-annealed samples at 240 °C and 320 °C, respectively. Noted, through the thermal annealing at 240 °C and voltage gating at ± 3 V, the Ta/CoFeB/HfO_x heterostructures enable the nonvolatile, reversible and bipolar control of SOT efficiency, and can implement electric field-controlled devices with low power consumption.

4. Conclusion

In conclusion, we have experimentally investigated the electric field effect and SOT efficiency in annealed Ta/CoFeB/HfO_x heterostructures. The annealing process significantly influences the magnetic properties, with higher annealing temperatures resulting in reduced H_c and M_s . The damping-like effective field efficiency also increases with higher annealing temperatures, peaking at approximately 320 °C, and an 80% field-free magnetization switching ratio was achieved. The enhanced SOT efficiency is attributed to interfacial mechanisms such as enhanced spin-orbit coupling strength, and an increased oxidized state for Co and Fe. Moreover, gating measurements reveal that the SOT efficiency can be reversibly and bidirectionally modulated by gate voltages, with different degree of responses observed for samples annealed at 240 °C and 320 °C due to their distinct oxidation levels. The ability to modulate SOT efficiency through electric field offers a useful way for the development of highly energy-efficient spintronic devices.

Data availability statement

All data that support the findings of this study are included within the article (and any supplementary files).

Acknowledgments

This work was supported by RIE2020 ASTAR AME IAF-ICP (Grant No. I1801E0030).

ORCID iDs

Shuo Wu  <https://orcid.org/0000-0002-4112-737X>

Gerard Joseph Lim  <https://orcid.org/0000-0003-2411-5841>

Wen Siang Lew  <https://orcid.org/0000-0002-5161-741X>

References

- [1] Cubukcu M *et al* 2018 Ultra-fast perpendicular spin-orbit torque MRAM *IEEE Trans. Magn.* **54** 1–4
- [2] Shao Q *et al* 2021 Roadmap of spin-orbit torques *IEEE Trans. Magn.* **57** 1–39
- [3] Nguyen M-H, Ralph D C and Buhrman R A 2016 Spin torque study of the spin Hall conductivity and spin diffusion length in platinum thin films with varying resistivity *Phys. Rev. Lett.* **116** 126601
- [4] Qiu X, Shi Z, Fan W, Zhou S and Yang H 2018 Characterization and manipulation of spin orbit torque in magnetic heterostructures *Adv. Mater.* **30** 1705699
- [5] Zhu L, Ralph D C and Buhrman R A 2018 Highly efficient spin-current generation by the spin Hall effect in $Au_{1-x}Pt_x$ *Phys. Rev. Appl.* **10** 31001
- [6] Kim J, Sinha J, Hayashi M, Yamanouchi M, Fukami S, Suzuki T, Mitani S and Ohno H 2013 Layer thickness dependence of the current-induced effective field vector in TaCoFeB/MgO *Nat. Mater.* **12** 240–5
- [7] Jin T, Law W C, Kumar D, Luo F, Wong Q Y, Lim G J, Wang X, Lew W S and Piramanayagam S N 2020 Enhanced spin-orbit torque efficiency in Pt/Co/Ho heterostructures via inserting Ho layer *APL Mater.* **8** 111111
- [8] Hasegawa K, Hibino Y, Suzuki M, Koyama T and Chiba D 2018 Enhancement of spin-orbit torque by inserting CoO_x layer into Co/Pt interface *Phys. Rev. B* **98** 20405
- [9] Amin V P, Zemen J and Stiles M D 2018 Interface-generated spin currents *Phys. Rev. Lett.* **121** 136805
- [10] Fan X, Celik H, Wu J, Ni C, Lee K-J, Lorenz V O and Xiao J Q 2014 Quantifying interface and bulk contributions to spin-orbit torque in magnetic bilayers *Nat. Commun.* **5** 3042
- [11] Qiu X, Narayanapillai K, Wu Y, Deorani P, Yang D-H, Noh W-S, Park J-H, Lee K-J, Lee H-W and Yang H 2015 Spin-orbit-torque engineering via oxygen manipulation *Nat. Nanotechnol.* **10** 333–8
- [12] Pachat R *et al* 2021 Multiple magnetoionic regimes in Ta/Co₂₀Fe₆₀B₂₀/HfO₂ *Phys. Rev. Appl.* **15** 64055
- [13] Pachat R *et al* 2022 Magneto-ionics in annealed W/CoFeB/HfO₂ thin films *Adv. Mater. Interfaces* **9** 2200690
- [14] Shimamura K, Chiba D, Ono S, Fukami S, Ishiwata N, Kawaguchi M, Kobayashi K and Ono T 2012 Electrical control of Curie temperature in cobalt using an ionic liquid film *Appl. Phys. Lett.* **100** 122402
- [15] Hwang H Y, Iwasa Y, Kawasaki M, Keimer B, Nagaosa N and Tokura Y 2012 Emergent phenomena at oxide interfaces *Nat. Mater.* **11** 103–13
- [16] Vaz C A F 2012 Electric field control of magnetism in multiferroic heterostructures *J. Phys.: Condens. Matter* **24** 333201
- [17] Matsukura F, Tokura Y and Ohno H 2015 Control of magnetism by electric fields *Nat. Nanotechnol.* **10** 209–20
- [18] Fassatoui A, Garcia J P, Ranno L, Vogel J, Bernard-Mantel A, Béa H, Pizzini S and Pizzini S 2020 Reversible and irreversible voltage manipulation of interfacial magnetic anisotropy in Pt/Co/Oxide multilayers *Phys. Rev. Appl.* **14** 64041
- [19] Chen L, Gmitra M, Vogel M, Islinger R, Kronseder M, Schuh D, Bougeard D, Fabian J, Weiss D and Back C H 2018 Electric-field control of interfacial spin-orbit fields *Nat. Electron.* **1** 350–5
- [20] Emori S, Bauer U, Woo S and Beach G S D 2014 Large voltage-induced modification of spin-orbit torques in Pt/Co/GdO_x *Appl. Phys. Lett.* **105** 222401
- [21] Wu S, Jin T L, Tan F N, Ang C C I, Poh H Y, Lim G J and Lew W S 2023 Enhancement of spin-orbit torque in Pt/Co/HfO_x heterostructures with voltage-controlled oxygen ion migration *Appl. Phys. Lett.* **122** 122403
- [22] Fan Y *et al* 2016 Electric-field control of spin-orbit torque in a magnetically doped topological insulator *Nat. Nanotechnol.* **11** 352–9
- [23] Yan Y *et al* 2016 Strong electrical manipulation of spin-orbit torque in ferromagnetic heterostructures *Adv. Electron. Mater.* **2** 1600219
- [24] Nozaki T, Tamaru S, Konoto M, Nozaki T, Kubota H, Fukushima A and Yuasa S 2021 Large voltage-induced coercivity change in Pt/Co/CoO/amorphous TiO_x structure and heavy metal insertion effect *Sci. Rep.* **11** 21448
- [25] Vermeulen B F, Swerts J, Couet S, Popovici M, Radu I P, Van de Vondel J, Temst K, Groeseneken G and Martens K 2020 Electronic voltage control of magnetic anisotropy at room temperature in high *k* SrTiO₃/Co/Pt trilayer *Phys. Rev. Mater.* **4** 114415
- [26] Liu R H, Lim W L and Urazhdin S 2014 Control of current-induced spin-orbit effects in a ferromagnetic heterostructure by electric field *Phys. Rev. B* **89** 220409
- [27] Song C, Cui B, Li F, Zhou X and Pan F 2017 Recent progress in voltage control of magnetism: materials, mechanisms, and performance *Prog. Mater. Sci.* **87** 33–82
- [28] Bekele Z A, Meng K, Miao J, Xu X and Jiang Y 2018 Modulated spin orbit torque via controlling the oxidation level of Ti in Pt/Co/TiO_x heterostructures *Solid State Commun.* **284–286** 5–10
- [29] Hayashi M, Kim J, Yamanouchi M and Ohno H 2014 Quantitative characterization of the spin-orbit torque using harmonic Hall voltage measurements *Phys. Rev. B* **89** 144425
- [30] Feng G, Zhang J, Liu J, Yang X, Chen X and Yu G 2022 Different oxygen migration behaviors at CoFe/MgO and CoFe/HfO₂ interfaces and their effects on the magnetic anisotropy *AIP Adv.* **12** 15222
- [31] Wells A W J, Shepley P M, Marrows C H and Moore T A 2017 Effect of interfacial intermixing on the Dzyaloshinskii-Moriya interaction in Pt/Co/Pt *Phys. Rev. B* **95** 54428
- [32] Zhu Z, Zhao B, Zhu W, Tang M, Ren Y, Jin Q Y and Zhang Z 2018 Annealing effect and interlayer modulation on magnetic damping of CoFeB/interlayer/Pt thin films *Appl. Phys. Lett.* **113** 222403

- [33] Meng H, Lum W H, Sbiaa R, Lua S Y H and Tan H K 2011 Annealing effects on CoFeB-MgO magnetic tunnel junctions with perpendicular anisotropy *J. Appl. Phys.* **110** 33904
- [34] Belmeguenai M, Aitoukaci K, Zighem F, Gabor M S, Petrisor T Jr, Mos R B and Tiusan C 2018 Investigation of the annealing temperature dependence of the spin pumping in $\text{Co}_{20}\text{Fe}_{60}\text{B}_{20}/\text{Pt}$ systems *J. Appl. Phys.* **123** 113905
- [35] Feng X, Yao J, Cui Y, Zhang P, Bai Q, Xi L, Cao J, Xue D and Fan X 2021 Impact of trace amounts of interfacial oxidation on the spin-orbit torque in the Co/Pt heterostructures *Appl. Phys. Lett.* **118** 132410
- [36] Haku S, Musha A, Gao T and Ando K 2020 Role of interfacial oxidation in the generation of spin-orbit torques *Phys. Rev. B* **102** 24405
- [37] Kageyama Y, Tazaki Y, An H, Harumoto T, Gao T, Shi J and Ando K 2023 Spin-orbit torque manipulated by fine-tuning of oxygen-induced orbital hybridization *Sci. Adv.* **5** eaax4278
- [38] Gilbert D A, Grutter A J, Arenholz E, Liu K, Kirby B J, Borchers J A and Maranville B B 2016 Structural and magnetic depth profiles of magneto-ionic heterostructures beyond the interface limit *Nat. Commun.* **7** 12264
- [39] Hirai T, Hibino Y, Hasegawa K, Kohda M, Koyama T and Chiba D 2020 Voltage control of spin-orbit torque in Pd/Co/Pd/HfO_x *Appl. Phys. Express* **13** 123005
- [40] Endo M, Kanai S, Ikeda S, Matsukura F and Ohno H 2010 Electric-field effects on thickness dependent magnetic anisotropy of sputtered MgO/Co₄₀Fe₄₀B₂₀/Ta structures *Appl. Phys. Lett.* **96** 212503
- [41] Suwardy J, Nawaoka K, Cho J, Goto M, Suzuki Y and Miwa S 2018 Voltage-controlled magnetic anisotropy and voltage-induced Dzyaloshinskii-Moriya interaction change at the epitaxial Fe(001)/MgO(001) interface engineered by Co and Pd atomic-layer insertion *Phys. Rev. B* **98** 144432
- [42] Maruyama T *et al* 2009 Large voltage-induced magnetic anisotropy change in a few atomic layers of iron *Nat. Nanotechnol.* **4** 158–61
- [43] Nakamura K, Akiyama T, Ito T, Weinert M and Freeman A J 2010 Role of an interfacial FeO layer in the electric-field-driven switching of magnetocrystalline anisotropy at the Fe/MgO interface *Phys. Rev. B* **81** 220409